

Lyapunov Modes in Hard-Disk Systems

February 9, 2020

Jean-Pierre Eckmann^{1,2}, Christina Forster³,

Harald A. Posch³, Emmanuel Zabey¹

¹ Département de Physique Théorique,

² Section de Mathématiques,

Université de Genève, Switzerland

³ Institute for Experimental Physics, University of Vienna, Austria

Abstract

We consider simulations of a 2-dimensional gas of hard disks in a rectangular container and study the Lyapunov spectrum near the vanishing Lyapunov exponents. To this spectrum are associated “eigen-directions”, called Lyapunov modes. We carefully analyze these modes and show how they are naturally associated with vector fields over the container. We also show that the Lyapunov exponents, and the coupled dynamics of the modes (where it exists) follow linear laws, whose coefficients only depend on the density of the gas, but not on aspect ratio and very little on the boundary conditions.

1 Introduction

In this paper, we study the Lyapunov spectra of two-dimensional hard-disk systems and, in particular, the associated “Lyapunov modes” [1, 2]. Recently, this topic has received considerable attention [3, 4, 5, 6, 7, 8]. The purpose of our work is to clarify some issues concerning the classification of these modes and the proper interpretation of their dynamics.

The Lyapunov *exponents* describe the rates of exponential growth, or decay, of infinitesimal phase-space perturbations, and are taken to be ordered according to $\lambda^{(1)} > \lambda^{(2)} > \dots > \lambda^{(\ell)}$.¹ Because of the Hamiltonian nature of the problem, they come in conjugate pairs,

$$\lambda^{(j)} = -\lambda^{(\ell-j+1)}.$$

¹ ℓ is at most the dimension of the phase space.

At any point ξ in phase space, dynamical-system theory associates with each Lyapunov exponent $\lambda^{(i)}$ a subspace $E^{(i)}(\xi)$ with the following properties:

$$E^{(i)}(\xi) \subset E^{(i-1)}(\xi), \quad i = 2, \dots, \ell.$$

$E^{(i)}(\xi)$ is the (linear) space of those perturbations of the initial condition ξ whose growth rate is bounded from above by $\lambda^{(i)}$.

Hard-disk systems are believed to be hyperbolic (apart from some conserved quantities, see below), and partial results in this direction have been obtained by Simányi and Szász [9]. Based on numerical evidence, we take this property for granted. Then, the Lyapunov *modes* are closely related to the spaces $E^{(i)}$ and are obtained as follows: at time $t = 0$, we take n orthogonal tangent vectors at ξ and, applying to them the tangent-space dynamics² for a long-enough time t , they are mapped onto n vectors which, generally, are not orthogonal but still span an n -dimensional subspace $S_n(t)$. If, instead of n , we consider only $n - 1$ vectors, they similarly span an $n - 1$ dimensional subspace $S_{n-1}(t)$, such that $S_{n-1}(t) \subset S_n(t)$. The “missing” normalized component orthogonal to $S_{n-1}(t)$ will be called the n^{th} **Lyapunov mode**. It should be noted that, when the Lyapunov exponents are d -fold degenerate, only the subspace corresponding to all d of them is well defined³. The main idea of our full classification of Lyapunov exponents and their modes is based on this simple observation.

The study of Lyapunov modes [2, 8] has revealed interesting spatial structures which we will define later but which come in two types: *localized structures* associated with the large positive and negative Lyapunov exponents, and *smooth delocalized structures* of wave-like type for exponents close to zero [1, 8]. The exponents associated with the latter are degenerate and give rise to a step-like appearance of the Lyapunov spectrum as is shown, for example, in Fig. 1.

The discovery of these structures has led to several studies [3, 4, 5, 6, 7] which go some way in explaining their origin and their dynamics. In this paper, we show how they are related to the symmetries of the container in which the particles move (including the boundary conditions). At the same time we obtain a classification of the degeneracies of the Lyapunov exponents near zero. This classification allows to view the so-called “mode dynamics” from a new geometrical perspective.

The paper starts with a summary of results, passes through a precise definition of the Lyapunov modes, and then describes them as vector fields. In Sec. 5 these vector fields are classified, and their dynamics is studied in Sec. 6. The last sections deal with the density dependence and with hydrodynamic aspects.

²See Section 2 for details.

³In this, and many other aspects, the theory of Lyapunov exponents is very similar to that of matrices.

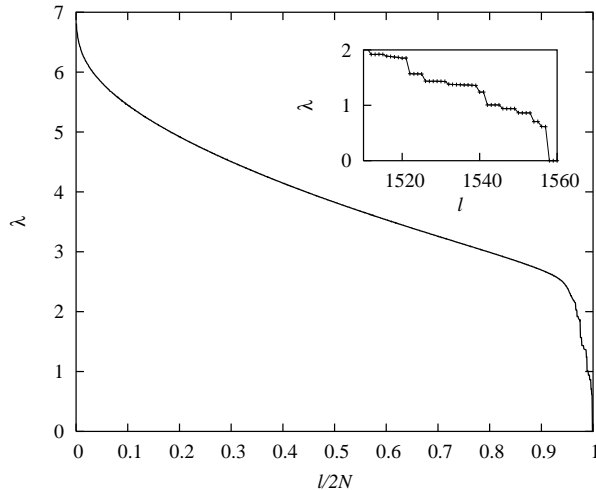


Figure 1: Lyapunov spectrum for $N = 780$ hard disks at a density $\rho \equiv N/(L_x L_y) = 0.8$ in a rectangular periodic box with an aspect ratio $L_y/L_x = 0.867$. The insert provides a magnified view of the mode regime. l is the Lyapunov index numbering the exponents.

2 Notation and summary of results

We consider a system of N hard disks of diameter σ and mass m moving in a two-dimensional rectangular container with sides of lengths L_x and L_y . At this point, we do not need to specify the boundary conditions.⁴ The phase space of such a system is

$$X = \mathbf{R}^{2N} \times ([0, L_x] \times [0, L_y])^N,$$

and a phase point ξ in X is

$$\xi = (p, q) = (p_1, \dots, p_N, q_1, \dots, q_N).$$

When necessary, we will write $q_i = (q_{i,x}, q_{i,y})$ to distinguish the two position components of particle i , and similarly for the momenta. The dynamics of the system is that of free flight, interrupted by elastic binary collisions. If ξ_0 is the state of the system at time 0, then $\xi_t = \Phi^t(\xi_0)$ is the state at time t , where $\Phi^t : X \rightarrow X$ defines the flow.

Apart from issues of differentiability, which will be addressed when we describe the numerical implementation in Section 3, we call $D\Phi^t$ the tangent flow. Informally speaking, it is a $4N \times 4N$ matrix of partial derivatives and can be thought of as the first-order term (in ε) in an expansion of the perturbed flow,

$$\Phi^t(\xi_0 + \varepsilon \delta \xi) = \Phi^t(\xi_0) + \varepsilon D\Phi^t|_{\xi_0} \cdot \delta \xi + \mathcal{O}(\varepsilon^2).$$

⁴We will consider reflecting and periodic boundary conditions.

The vector $\delta\xi$ lies in the tangent space TX (at ξ_0) to the manifold X ; in our case $TX(\xi_0) = \mathbf{R}^{4N}$. The multiplicative ergodic theorem of Oseledec [10, 11] states that under suitable conditions on Φ^t , which we assume to be true, the following holds:

Theorem: *For almost every $\xi \in X$ the tangent space splits into a sequence of spaces*

$$TX(\xi) = E^{(1)}(\xi) \supset E^{(2)}(\xi) \supset \cdots \supset E^{(\ell)}(\xi) \supset E^{(\ell+1)}(\xi) = \emptyset,$$

such that for $i = 1, \dots, \ell$,

$$\lim_{t \rightarrow \infty} \left(D\Phi^t|_{\xi}^* \cdot D\Phi^t|_{\xi} \right)^{1/(2t)} \delta\xi = e^{\lambda^{(i)}} \delta\xi,$$

for $\delta\xi \in E^{(i)}(\xi) \setminus E^{(i+1)}(\xi)$.⁵ The spaces $E^{(i)}(\xi)$ are covariant: $D\Phi^t|_{\xi} E^{(i)}(\xi) = E^{(i)}(\xi_t)$.

The dimension of $E^{(i)}(\xi) \setminus E^{(i+1)}(\xi)$ is called multiplicity of the exponent $\lambda^{(i)}$. When needed, we also use the notation

$$\lambda_1 \geq \lambda_2 \geq \cdots \geq \lambda_{4N}$$

to denote the Lyapunov exponents repeated with multiplicities, where the index is referred to as the Lyapunov index. This notation is more adequate for describing numerical methods of measurement, in which tangent-space dynamics is probed by a set of vectors. The set of Lyapunov exponents, also called the Lyapunov spectrum, is (almost surely) independent of ξ if the system is ergodic.

Here, we focus on rectangular boxes with **periodic** boundary conditions. Narrow systems ($L_y < 2\sigma$) or systems with reflecting boundaries have a very similar Lyapunov spectrum, but some exponents found in the periodic case are either absent, or appear with smaller multiplicities. We shall treat such systems in Sec. 5.3 but concentrate, until then, on the “general” periodic case. However, it should be noted that systems with reflecting boundaries give important information on the relation between the vanishing and the small Lyapunov exponents (see Ex. 5 below).

The Lyapunov exponents near zero are found to be proportional to the wave numbers of the system

$$k_{(n_x, n_y)} = \sqrt{\left(\frac{2\pi}{L_x} n_x\right)^2 + \left(\frac{2\pi}{L_y} n_y\right)^2}, \quad n_x, n_y = 0, 1, \dots, \quad (1)$$

and have the following properties:

Lyapunov Spectrum: *For gases of hard disks, the Lyapunov exponents near zero are fully de-*

⁵That is, the vector $\delta\xi$ stretches (or contracts) with rate $\lambda^{(i)}$ provided it is in $E^{(i)}$ but not in $E^{(i-1)}$.

terminated by two (positive) constants, c_L and c_T . For small-enough $\mathbf{n} = (n_x, n_y)$, these exponents lie on two straight lines.⁶

- 1) *Transverse branch (T)* : $\lambda = \pm c_T k_{\mathbf{n}}$, with multiplicity 4 (2 if either n_x or n_y is zero)
- 2) *Longitudinal branch (L)* : $\lambda = \pm c_L k_{\mathbf{n}}$, with multiplicity 8 (4 if either n_x or n_y is zero)

The multiplicities of both branches will be explained by simple geometric observations in Sec. 5.2. While the linear laws resemble the square roots of the eigenvalues of a Laplacian in the box, we have no explanation beyond those already given in Ref. [3]. (The square root is related to the symplectic nature of the problem.) Additional degeneracies arise in square systems and may accidentally appear also for specific aspect ratios L_y/L_x .

The Lyapunov modes described in the Introduction are closely related to the $E^{(i)}$ subspaces of Oseledec's theorem: in some “ideal” cases they would (for every ξ) be spanning vectors of the subspaces $E^{(i)}(\xi) \setminus E^{(i+1)}(\xi)$. We discuss this issue in Sec. 3.2. For now we assume that for each Lyapunov exponent $\lambda^{(i)}$ of multiplicity d_i , and each phase point ξ , we have a set of d_i independent tangent vectors that we call *the Lyapunov modes associated with the exponent $\lambda^{(i)}$* . These d_i vectors span a subspace that we denote by $M^{(i)}(\xi)$.

We next explain how to visualize a mode [12, 8]. Fix $\xi = (p, q) \in X$, and let $\delta\xi$ be a Lyapunov mode of $TX(\xi)$. The vector $\delta\xi = (\delta p, \delta q)$ has $4N$ components, $2N$ associated with the momenta and $2N$ with the positions. Consider, for example, the q components, $\delta q_1, \dots, \delta q_N$, where each δq_j is in \mathbf{R}^2 (corresponding to the infinitesimal x and y displacements of q_j , $j = 1, \dots, N$). By drawing the perturbation vectors δq_j at the positions q_j of the particles in the box, one obtains a field of vectors as is shown in Fig. 2. For dense-enough fluids we obtain a vector field in every point of the box by interpolating between the particles.

It has been observed that for those Lyapunov exponents close to zero, this vector field is well approximated by trigonometric functions of the spatial coordinates x and y [1, 8]. In particular, the number of nodes (n_x, n_y) of the vector field determines a wave number $k_{\mathbf{n}}$. We then say that $\delta\xi$ is a mode of wave number $k_{\mathbf{n}}$. Our second main result is:

Mode Classification: *The subspaces $M^{(i)}(\xi)$ belonging to Lyapunov exponents close to zero fall into two categories:*

- 1) *Transverse branch: modes associated with a Lyapunov exponent $\pm c_T k_{\mathbf{n}}$ are divergence-free periodic fields of wave number $k_{\mathbf{n}}$.*
- 2) *Longitudinal branch: The modes associated with the Lyapunov exponent $\pm c_L k_{\mathbf{n}}$ are of two types:*

⁶For both the longitudinal and transverse modes the linear k dependence of λ is only the first term of an expansion in powers of k [8], $\lambda = ck + c_2 k^2 \dots$. For positive λ , c_2 is positive, but small.

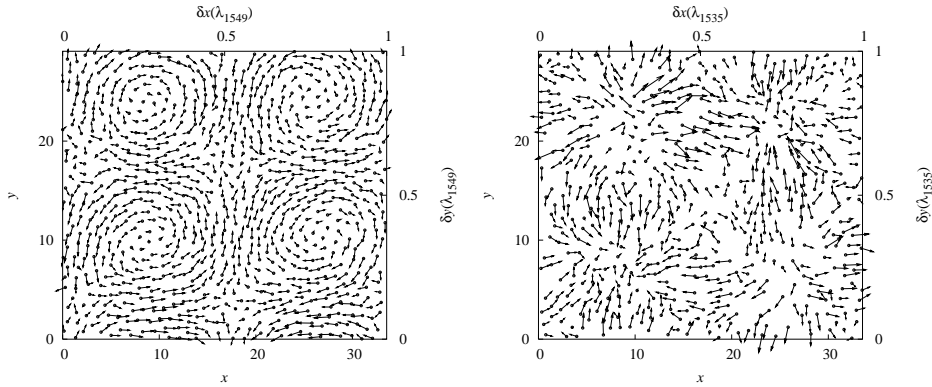


Figure 2: Modes for the 780-disk system with periodic boundaries characterized in Fig. 1. Left: Transverse mode $T(1,1)$ belonging to λ_{1549} . Right: Longitudinal mode for λ_{1535} belonging to an LP pair $LP(1,1)$.

- (i) *Half of them are irrotational periodic vector fields of wave number k_n (called L-modes);*
- (ii) *The others are scalar modulations with wave number k_n of the momentum field, (called P or momentum modes).*

The L and the P-modes turn out to be paired: the P-mode has components $p_i A(q_i)$ and the corresponding L-mode has components $\nabla A(q_i)$, where A is a scalar function, see (8). In the following, we refer to an L-mode and its corresponding P-mode as an **LP pair**. We will give more details on this relation below. Partial results in this direction have been obtained in Refs. [4, 7].

An interesting question, which is related to some hydrodynamic aspects of the fluid, is an apparent propagation of the L and P-modes in physical space. It is a consequence of the motion of the tangent vectors in the subspaces $M^{(i)}(\xi_t)$, to which we refer as *mode dynamics*. It will be described in detail in Section 6. We note that this motion is not only determined by the tangent flow, but also by the re-orthonormalization process part of the algorithm for the simulation. Mode dynamics was observed early on [2, 12], but attempts to compute the propagation velocities are still scarce and, at present, only work for low densities [5, 7]. Here, we give a more precise definition and provide numerical results.

Mode Dynamics: *In an $M^{(i)}$ space of Longitudinal and P-modes, the mode dynamics couples LP pairs. When restricted to the two-dimensional subspace spanned by a given LP pair, it reduces to a rotation at constant angular velocity ω_n which is proportional to the wave number k_n ,*

$$\omega_n = v k_n ,$$

where v has the dimension of a velocity.

In the remainder of the paper we state these results more precisely and give details about how they are obtained. They are of two types: First, a theoretical description of the modes, which is based on the symmetries of the system. Second, a detailed account of the numerical algorithms necessary to substantiate our claims (the difficulty being the decomposition of the d_i dimensional spaces $M^{(i)}(\xi)$).

3 Tangent-space dynamics

The dynamics of hard disks consists of phases of free flight interrupted by instantaneous elastic collisions. We denote the map for free flights of duration τ by F^τ , and the collision map by C . Then, the evolution of an initial state, ξ_0 , is given by

$$\xi_t = F^{\tau_n} \circ \cdots \circ C \circ F^{\tau_2} \circ C \circ F^{\tau_1} \xi_0, \quad (2)$$

where τ_1, \dots, τ_n are the time intervals between successive collisions. The *tangent-space dynamics* of an infinitesimal perturbation $\delta\xi_0$ of ξ_0 is given by the tangent map of the flow (2) :

$$\delta\xi_t = DF^{\tau_n}|_{\xi_n^+} \cdots DC|_{\xi_2^-} \cdot DF^{\tau_2}|_{\xi_1^+} \cdot DC|_{\xi_1^-} \cdot DF^{\tau_1}|_{\xi_0} \delta\xi_0,$$

where ξ_k^- denotes the state just before the k^{th} collision, and $\xi_k^+ = C(\xi_k^-)$ is the state immediately after.⁷ Here, $DF^\tau|_{\xi_k}$ and $DC|_{\xi_k}$ are $4N \times 4N$ symplectic matrices. For the sake of simplicity, the flow is also called Φ^t : namely $\Phi^t(\xi_0) = \xi_t$, and we often write $\delta\xi_t = D\Phi^t|_{\xi_0} \cdot \delta\xi_0$. By convention, if t is a collision time, $\delta\xi_t$ denotes a tangent vector immediately before that collision.

3.1 Numerical procedure and Lyapunov modes

Extensive numerical simulations are used to establish the classification and dynamics of the modes. Here, we briefly summarize our algorithm [13, 2] and provide a precise definition of the Lyapunov modes we observe. It is well known that the exponential growth rate of a typical k -dimensional volume element is given by $\lambda_1 + \cdots + \lambda_k$,

$$\lambda_1 + \cdots + \lambda_k = \lim_{t \rightarrow \infty} \frac{1}{t} \log \|\delta\xi_t^1 \wedge \cdots \wedge \delta\xi_t^k\|. \quad (3)$$

If the tangent vectors $\delta\xi^1, \dots, \delta\xi^k$ are linearly independent at time zero, they will remain so, because the tangent flow is time reversible. Orthogonality is not preserved by the tangent flow, because, generally, $D\Phi^t$ is not orthogonal. However, (3) still holds if the vectors $\delta\xi_t^1, \dots, \delta\xi_t^k$ are replaced by a (Gram-Schmidt) orthogonalized set of vectors $\delta\eta_t^1, \dots, \delta\eta_t^k$.⁸ It takes thus the simpler form

$$\lambda_1 + \cdots + \lambda_k = \lim_{t \rightarrow \infty} \frac{1}{t} \sum_{i=1}^k \log \|\delta\eta_t^i\|. \quad (4)$$

⁷We disregard problems of differentiability which appear for the (rare) tangent collisions.

⁸ $\delta\eta_t^j = \delta\xi_t^j - \sum_{i=1}^{j-1} (\delta\xi_t^j \cdot \delta\xi_t^i) / (\|\delta\xi_t^i\|^2) \delta\xi_t^i$

Since (4) holds for every $k \leq 4N$, the exponent λ_k turns out to be equal to the growth rate of the k^{th} orthogonalized vector $\delta\eta_t^k$.

The numerical method of Benettin *et al.*[14] and Shimada *et al.*[15] – and indeed any algorithm – is based on this construction, although its basic objects are not the $\delta\eta_t^k$ vectors. As time increases, they all would get exponentially close to the most-unstable direction, become numerically indistinguishable, and diverge. Instead of orthogonalizing *once* at time t , the tangent dynamics is applied to a set of tangent vectors, which are periodically replaced by an orthogonalized set, that we denote by $\delta\gamma_t^1, \dots, \delta\gamma_t^k$. The modified dynamics is therefore that of an orthogonal frame [13, 2]. Clearly, (4) is still valid, if $\delta\eta_t^k$ is replaced by $\delta\gamma_t^k$. The k^{th} Lyapunov mode (or Lyapunov vector) at time t is, by definition, the vector $\delta\gamma_t^k$, and it is associated with the exponent λ_k .

The algorithm we use in our numerical work [13, 2] is based on the principles just outlined. Throughout, reduced units are used, for which the particle mass m , the disk diameter σ , and the kinetic energy per particle, K/N , are unity. With this choice, the unit of time is $(m\sigma^2 N)/K)^{1/2}$. For hard-disk systems in thermodynamic equilibrium, to which we restrict our considerations, the temperature is an irrelevant parameter, since there is no potential energy, and the dynamics strictly scales with $\sqrt{K/N}$. It suffices to consider a single isotherm, and the density, defined by $\rho = N/V$, is the only relevant macroscopic parameter. Here, $V = L_x L_y$ is the area of the (rectangular) simulation box whose sides are L_x and L_y in the x and y directions, respectively. The aspect ratio is defined by $A = L_y/L_x$. All our numerical examples are for densities $\rho \leq 0.8$ characteristic of dense or dilute (if $\rho < 0.1$) hard disk gases.

3.2 Relation to ergodic theory

The definition of the Lyapunov modes given above does not show why these vectors should be related to the $E^{(i)}(\xi)$ subspaces defined by Oseledec' theorem. For this to happen, additional properties of the dynamical system are needed: Namely, that the system has well-defined local stable and unstable manifolds, and a system of contracting cones.

Such properties are known for special systems, such as the Sinai billiard, and we assume here that they hold for the hard-core gas as well. As already advocated in Ref. [11], what matters from a physicist's point of view is that the numerical studies behave as if this were true. In that case, the k^{th} mode will align with the tangent space to the corresponding unstable manifold. For each ξ , we denote by $S^{(i)}(\xi)$ the unstable subspace, in which the growth rate is at least $\lambda^{(i)}$. This subspace is spanned by the modes whose associated exponent is at least $\lambda^{(i)}$. The subspaces $S^{(i)}$ satisfy

$$S^{(i)}(\xi) \subset S^{(i+1)}(\xi),$$

and are covariant.⁹ The relation between these unstable subspaces and those of Oseledec goes

⁹Since $\bar{m} = \frac{1}{2}(\ell + 1)$ is the index of the exponent $\lambda^{(\bar{m})} = 0$, the subspace $S^{(\bar{m}+1)}$ is the tangent subspace to the

as follows: Let k be the index of a positive exponent $\lambda^{(k)} > 0$. Inside a covariant subspace $S^{(k)}$, growth takes place at a rate that is at least $\lambda^{(k)}$. If we make the dynamics go *backwards in time*, the decay rate in the same subspace is at least $-\lambda^{(k)} = \lambda^{(\ell-k+1)}$, exactly as in an $E^{(\ell-k+1)}$ space. Now we use that our system is invariant under time-reversal, that is, backward dynamics is the same as forward dynamics when all the velocities in the initial condition are reversed. Defining $J : (p, q) \mapsto (-p, q)$, this latter property is

$$\Phi^{-t} = J \circ \Phi^t \circ J,$$

from which we obtain

$$S^{(i)}(\xi) = E^{(\ell-i+1)}(J\xi).$$

Measured modes on a phase point ξ are thus spanning vectors of Oseledec's subspaces of another point $J\xi$. However, in the classification of the modes we shall introduce in the sequel, this makes little difference, for the modes over $\xi = (p, q)$ are identical to those over $J\xi = (-p, q)$.

4 Tangent vectors as vector fields

The components of a tangent vector $\delta\xi = (\delta p, \delta q)$ are the perturbation components of the positions and velocities of all particles. As a graphical representation of such a vector, we show on the left-hand side of Fig. 3 the instantaneous positional perturbations of all particles *at their positions* in physical space, where the arrows indicate the directions and strengths. It belongs to a Lyapunov exponent λ_{1546} indicated by the enlarged circle in Fig. 5. A qualitatively identical figure is obtained, if the positional displacements of all particles are replaced by their momentum displacements, as we shall explain below. Thus, this figure is a complete representation of the Lyapunov vector $\delta\xi = (\delta p, \delta q)$ belonging to λ_{1546} in Fig. 5. The transverse modes for λ_{1549} on the left-hand side of Fig. 2, and for λ_{1548} at the bottom-left corner of Fig. 6, are other examples of transverse modes belonging to the same degenerate exponent.

We interpret the left-hand side of Fig. 3 as a two-dimensional *vector field* φ which – up to a constant phase – is well described by

$$\begin{pmatrix} \varphi_x(x, y) \\ \varphi_y(x, y) \end{pmatrix} = \begin{pmatrix} \alpha_1 \cos(k_x x) \sin(k_y y) \\ -\alpha_2 \sin(k_x x) \cos(k_y y) \end{pmatrix},$$

where $k_x = \frac{2\pi}{L_x}$ and $k_y = \frac{2\pi}{L_y}$, and α_1, α_2 are two constants. For this reason, we assign the node numbers $(n_x, n_y) = (1, 1)$ to this mode.

unstable manifold. We do not need to assume that the $S^{(i)}$ spaces are well defined for every i , but only a few “steps” around zero, that is, for those i for which $|\bar{m} - i| \ll \ell$.

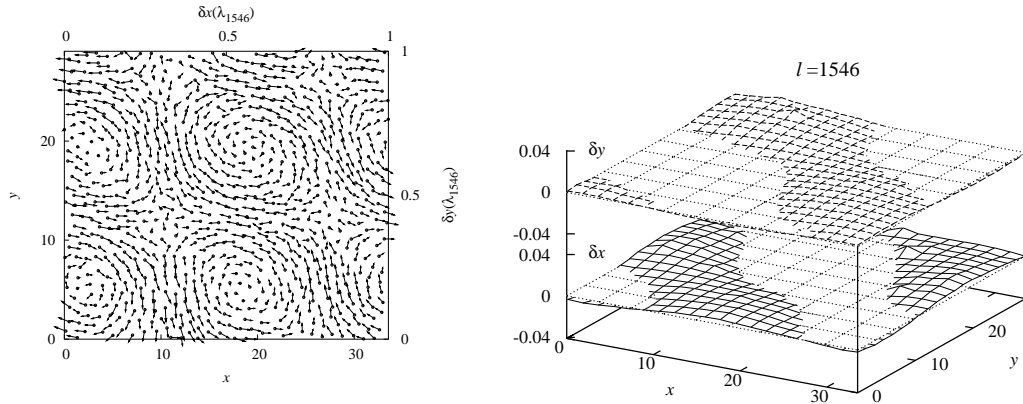


Figure 3: The transverse mode $T(1,1)$ for λ_{1546} of Fig. 5. Left: Interpretation as a vector field; Right: Alternative representation as periodic spatial patterns of the position perturbations δx_i and δy_i of the particles, which emphasizes the wave vector parallel to a diagonal of the simulation box.

To be more precise, let $r = (x, y) \in [0, L_x] \times [0, L_y]$. We say that a two-dimensional smooth vector field $\varphi = (\varphi_x, \varphi_y)$ over the position space, is *sampled* by the infinitesimal displacements δq of the N disks at their reference positions q , when

$$\varphi(q_j) = \delta q_j, \text{ for all } j = 1, \dots, N.$$

Thinking of a tangent vector in terms of an associated vector field is meaningful if there are “sufficiently” many particles to sample the field on a typical length scale of its variation. Once this condition breaks down for larger exponents, as it will for large-enough k , the modes disappear¹⁰, and so do the steps in the Lyapunov spectrum. In the following we use a notation which does not distinguish between tangent vectors and their two-dimensional vector fields.

4.1 Stable and unstable perturbations

Because of the symplectic structure of the tangent-space dynamics the Lyapunov exponents come in pairs of opposite signs. The associated Lyapunov vectors are also paired : if $\delta \xi = (\delta p, \delta q)$ is a Lyapunov vector for λ , then $\delta \xi' = (\delta q, -\delta p)$ is a Lyapunov vector for $-\lambda$. Hard-disk systems have an additional structure, characteristic of hyperbolic Hamiltonian systems [16, 17, 3], which considerably simplifies the analysis of Lyapunov vectors: *Unstable* perturbations ($\lambda > 0$) have

¹⁰and the sampled vector field is ill-defined.

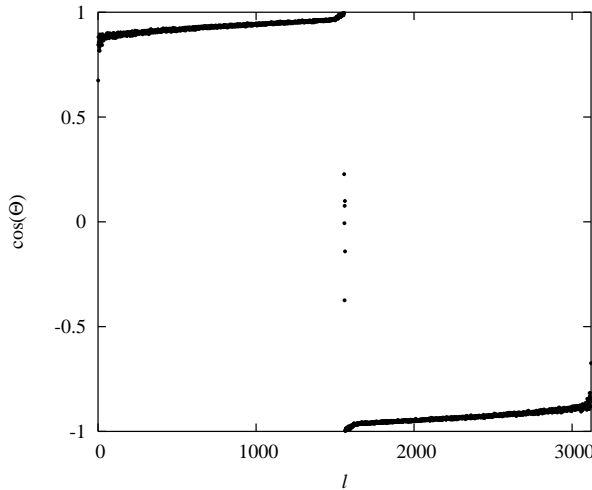


Figure 4: Value of $\cos(\Theta) = (\delta q \cdot \delta p) / (|\delta q| \cdot |\delta p|)$, as a function of the Lyapunov index l for an instantaneous configuration of the system characterized in Fig. 1. Here, Θ is the angle between the $2N$ -dimensional vectors of the perturbation components of all particle positions and velocities for a Lyapunov vector ξ_l . For the small positive exponents, for which $l < 2N - 2 = 1558$, this angle vanishes, for the small negative exponents, for which $l > 2N + 3 = 1563$, it is equal to π . For the six zero modes, $1558 \leq l \leq 1563$, the angle lies between these limiting values.

the form¹¹

$$\delta p = C \cdot \delta q, \quad C > 0, \quad (5)$$

whereas the *stable* ($\lambda < 0$) perturbations are

$$\delta p = -C \cdot \delta q. \quad (6)$$

Our classification of the Lyapunov vectors can therefore be restricted to the δq part of the modes corresponding to positive exponents. If we can associate every measured exponent λ to a given δq , then we know that the exponent $\pm\lambda$ corresponds to the vector $(\pm C\delta q, \delta q)$. The conjugate behavior in Eqs. (5) and (6) is verified by computer simulations (Fig. 4).

5 Observation and description of the modes

In this section, we describe the Lyapunov spectrum near 0 and the corresponding modes, as they are measured in numerical experiments. In the two following subsections, we will explain how

¹¹The “constant” C has the units of [mass·time⁻¹] and depends on the physical parameters (mass of a particle, mean collision time) of the system. In numerical simulations, C can vary from a mode to another, and even on the same mode along time.

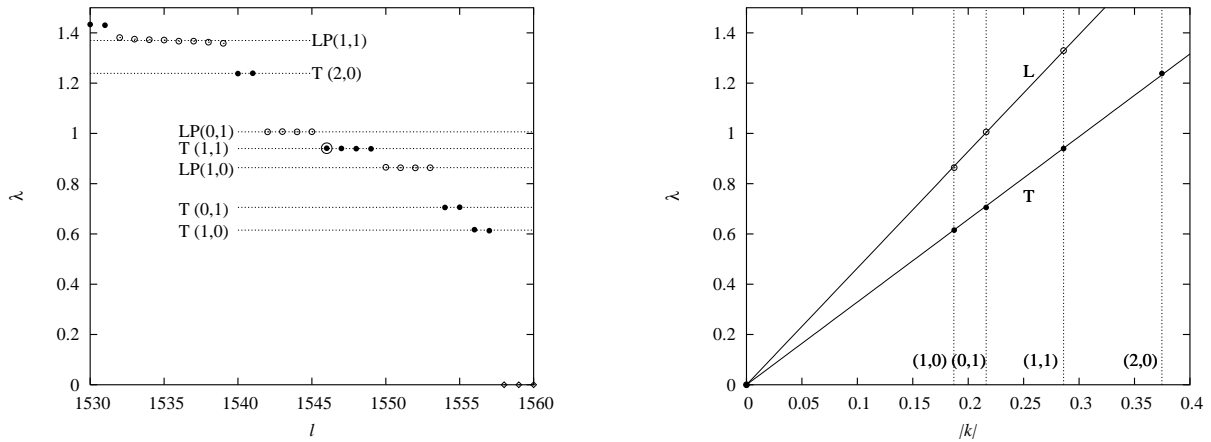


Figure 5: Lyapunov spectrum and “dispersion relations” for the 780-disk system characterized in Fig. 1, and the density $\rho = 0.8$. Left: Lyapunov exponents are ordered by size and repeated with multiplicities. The specially-marked point corresponds to the transverse mode shown in Fig. 3. Right: Lyapunov exponents as a function of their wave number. The respective labels L and T refer to the longitudinal and transverse branches.

these modes can be understood on the basis of symmetry breaking of “zero modes”.

We illustrate our assertions with the system already introduced in Fig. 1, which contains $N = 780$ particles in a rectangular periodic box with an aspect ratio $L_y/L_x = 0.867$. It corresponds to a hard-disk gas with a density $\rho = 0.8$, slightly below the fluid-to-solid phase transition density [13]. The left-hand side of Fig. 5 provides a magnified view of the smallest positive Lyapunov exponents for this system.¹² The exponents, ordered by size and repeated with their multiplicities, are plotted as a function of their index. Degenerate exponents with a multiplicity $d \geq 2$ appear therefore as “steps”. To account for the wave-like appearance of the modes, we associate with each Lyapunov vector a wave number $k_{(n_x, n_y)}$, as in (1), where the non-negative integers $\mathbf{n} = (n_x, n_y)$ count the nodes in the respective directions.¹³

When the small Lyapunov exponents are plotted as a function of their corresponding wave number, they all lie on two curves, sometimes referred to as “dispersion relations” [2, 8]. This is demonstrated on the right-hand side of Fig. 5. On this plot, degenerate exponents are represented by a single point. For reasons discussed below, the upper branch is called *longitudinal* (L), and the lower *transverse* (T). It is experimentally found that for a given wave number, the multiplicity of the L branch is twice that of the T branch, as mentioned already in Sec. 2.

¹²The conjugate negative exponents are not shown, see [2, 8].

¹³In many cases, the number of nodes is easy to determine, as in Fig. 3. To facilitate an objective identification of the wave vectors modes associated with larger exponents, which are noisier, Fourier-transforms are used.

5.1 Vanishing Lyapunov exponents

We start our description with the six modes associated with the six vanishing Lyapunov exponents, commonly referred to as *zero modes*. Four of them are induced by the homogeneity of space, and two are consequences of the homogeneity of time. They span a six-dimensional subspace $\mathcal{N}(\xi)$ of the tangent space, $TX(\xi)$, at any phase point ξ .¹⁴ These 6 zero modes play a fundamental role in understanding the nature of the modes associated with Lyapunov exponents close to zero.

In order to show which symmetries give rise to the zero modes, we list in Table 1 the six corresponding elementary transformations. This defines the six zero modes $\delta\xi_1$ to $\delta\xi_6$ in a notation that separates the x and y components of δp and δq . The vectors $\delta\xi_1$ and $\delta\xi_2$ correspond to a perturbation of the total momentum in the x and y directions, $\delta\xi_3$ and $\delta\xi_4$ to an (infinitesimal) uniform translation of the origin, $\delta\xi_5$ to a change of energy, and $\delta\xi_6$ to a change of the origin of time.

Transformation	Generator
$(p, q) \mapsto (p_x + \varepsilon 1, p_y, q_x, q_y)$	$\delta\xi_1 = (1, 0, 0, 0)$
$(p, q) \mapsto (p_x, p_y + \varepsilon 1, q_x, q_y)$	$\delta\xi_2 = (0, 1, 0, 0)$
$(p, q) \mapsto (p_x, p_y, q_x + \varepsilon 1, q_y)$	$\delta\xi_3 = (0, 0, 1, 0)$
$(p, q) \mapsto (p_x, p_y, q_x, q_y + \varepsilon 1)$	$\delta\xi_4 = (0, 0, 0, 1)$
$(p, q) \mapsto (p_x + \varepsilon p_x, p_y + \varepsilon p_y, q_x, q_y)$	$\delta\xi_5 = (p_x, p_y, 0, 0)$
$(p, q) \mapsto (p_x, p_y, q_x + \varepsilon p_x, q_y + \varepsilon p_y)$	$\delta\xi_6 = (0, 0, p_x, p_y)$

Table 1: Central subspace for the vanishing Lyapunov exponents. Notation : $1 = (1, 1, \dots, 1)$, and $0 = (0, 0, \dots, 0)$. All vectors have $4N$ components.

Two properties of $\mathcal{N}(\xi) = \text{Span}\{\delta\xi_1, \dots, \delta\xi_6\}$ will be important:

- $\mathcal{N}(\xi)$ is a covariant subspace of the tangent space. More precisely, $DC|_{\xi^-} : \mathcal{N}(\xi^-) \rightarrow \mathcal{N}(\xi^+)$ and $DF^\tau|_{\xi_t} : \mathcal{N}(\xi_t) \rightarrow \mathcal{N}(\xi_{t+\tau})$ are isomorphisms.
- A tangent vector $\delta\eta_0$ orthogonal to $\mathcal{N}(\xi_0)$ remains orthogonal under the tangent flow: $\delta\eta_t \perp \mathcal{N}(\xi_t)$.

These properties are easily verified by using the explicit Jacobians for the particle collisions, $DC|_\xi$, and for the free-streaming motion, $DF^\tau|_\xi$, as given in [13, 18, 2]. They mean that the Lyapunov subspace $\mathcal{N}(\xi)$ may be treated as an independent part of the tangent-space dynamics.

¹⁴It is important to keep in mind that $\mathcal{N}(\xi)$ really depends on ξ , see below.

Remark 1 The subspace $\mathcal{N}(\xi)$ can be further decomposed into three covariant subspaces $\mathcal{N}_x = \text{Span}\{\delta\xi_1, \delta\xi_3\}$, $\mathcal{N}_y = \text{Span}\{\delta\xi_2, \delta\xi_4\}$ and $\mathcal{N}_p = \text{Span}\{\delta\xi_5, \delta\xi_6\}$, each of which independently satisfies the properties listed for $\mathcal{N}(\xi)$. In systems with reflecting boundaries, only \mathcal{N}_p is present, while \mathcal{N}_x and \mathcal{N}_y are absent, because they are related to translation invariance. If only the x direction is periodic [6], the space of zero modes is reduced to $\mathcal{N}_x \oplus \mathcal{N}_p$.

5.2 Longitudinal, Transverse and P-modes

Following our argument of Sec. 4.1, we need only describe the δq part of the modes, knowing that the corresponding tangent vector is $(\pm C\delta q, \delta q)$. Therefore, we consider the three transformations (see Table 1)

$$\begin{aligned}\delta\xi_3 : (q_{x,j}, q_{y,j}) &\mapsto (q_{x,j} + \varepsilon, q_{y,j}) \\ \delta\xi_4 : (q_{x,j}, q_{y,j}) &\mapsto (q_{x,j}, q_{y,j} + \varepsilon) \\ \delta\xi_6 : (q_{x,j}, q_{y,j}) &\mapsto (q_{x,j} + \varepsilon p_{x,j}, q_{y,j} + \varepsilon p_{y,j}) ,\end{aligned}\tag{7}$$

associated to zero modes, and claim the following :

Modes Classification I: *Modes of wave number k_n are scalar modulations of (7) with wave number k_n . More precisely, they are obtained by replacing ε with $\varepsilon A(q_{x,j}, q_{y,j})$ in (7), where the real scalar function A is of the form*

$$A(x, y) = \sum_{|\ell|=n_x, |m|=n_y} c_{\ell,m} \exp(i(\ell k_x x + m k_y y)) ,$$

The space of such modulations has dimension 4 in general and dimension 2 if either n_x or n_y vanishes.

Example 2 We consider $\mathbf{n} = (1, 0)$, $(0, 1)$ and $(1, 1)$. We use the notation $c_x = \cos(k_x x)$, $s_x = \sin(k_x x)$, $c_y = \cos(k_y y)$ and $s_y = \sin(k_y y)$. A basis of the space of functions with wave number k_n is shown in Table 2. Of course, this choice fixes a constant phase for the sine and cosine functions.

\mathbf{n}	Function A	dim
$(1, 0)$	c_x, s_x	2
$(0, 1)$	c_y, s_y	2
$(1, 1)$	$c_x c_y, s_x c_y, c_x s_y, s_x s_y$	4

Table 2: Functions with wave number k_n

If the Lyapunov exponent were a function of k_n only, we would expect 12-fold degeneracy in Fig. 5, (resp. 6-fold if either n_x or $n_y = 0$), since each of the three perturbations of (7) can be

modulated by the four (resp. two) functions of Table 2. However, this degeneracy is broken into an 8+4 (resp. 4+2) structure:

Mode Classification II: *The Lyapunov vectors of wave number k_n have two possible Lyapunov exponents: $|\lambda| = c_T |k_n|$ or $|\lambda| = c_L |k_n|$, corresponding to the Transverse or Longitudinal branch of Fig. 5. The modes for these two branches are obtained as follows:*

- 1) *Transverse branch: transverse modes are obtained by combining the modulations of $\delta\xi_3$ and $\delta\xi_4$ in a divergence-free vector field. We denote by $T(\mathbf{n})$ the space of such vector fields.*
- 2) *Longitudinal branch:*
 - (i) *Longitudinal modes are irrotational vector fields one obtains by combining the modulations of $\delta\xi_3$ and $\delta\xi_4$. We denote the corresponding space by $L(\mathbf{n})$.*
 - (ii) *P-modes are modulations of $\delta\xi_6$, and we denote the corresponding subspace by $P(\mathbf{n})$.*

The three subspaces $T(\mathbf{n})$, $L(\mathbf{n})$ and $P(\mathbf{n})$ have dimension 4 (or dimension 2 if either n_x or n_y vanishes). We denote by $LP(\mathbf{n}) \equiv L(\mathbf{n}) \oplus P(\mathbf{n})$ the subspace corresponding to the Longitudinal branch. It has dimension 8 (4 if either n_x or n_y vanishes).

Remark 3 The divergence and curl of a vector field $\varphi = (\varphi_x, \varphi_y)$ are, of course,

$$\nabla \cdot \varphi = \partial_x \varphi_x + \partial_y \varphi_y, \quad \nabla \wedge \varphi = \partial_x \varphi_y - \partial_y \varphi_x.$$

Since every two-dimensional vector field uniquely decomposes into a sum of a divergence-free and an irrotational vector field, the spaces $L(\mathbf{n})$ and $T(\mathbf{n})$ span all possible two-dimensional vector fields of wave number k_n .

There is a simple way to build $P(\mathbf{n})$, $L(\mathbf{n})$ and $T(\mathbf{n})$ from the scalar modulations of Table 2. If A is a modulation of wave number k_n , then we have

$$pA \in P(\mathbf{n}), \quad \nabla A \in L(\mathbf{n}), \quad \nabla \wedge A \in T(\mathbf{n}), \quad (8)$$

where by definition

$$\nabla A = \begin{pmatrix} \partial_x A \\ \partial_y A \end{pmatrix}, \quad \nabla \wedge A = \begin{pmatrix} \partial_y A \\ -\partial_x A \end{pmatrix}.$$

This construction is also useful because it naturally defines what we shall call **LP pairs**, by which we denote a field of $L(\mathbf{n})$ and a field of $P(\mathbf{n})$ originating from the same scalar modulation, as in (8). We show below that LP pairs play an important role. Indeed, when only some of the modes are present because of the boundary conditions, LP pairs are never broken: both fields are present, or both are missing (see Sec. 5.3). We shall also see in Sec. 6 that the dynamics of the modes takes mostly place between LP pairs.

\mathbf{n}	Basis of $T(\mathbf{n})$	Basis of $L(\mathbf{n})$	Basis of $P(\mathbf{n})$
$(1, 0)$	$\begin{pmatrix} 0 \\ c_x \end{pmatrix}, \begin{pmatrix} 0 \\ s_x \end{pmatrix}$	$\begin{pmatrix} c_x \\ 0 \end{pmatrix}, \begin{pmatrix} s_x \\ 0 \end{pmatrix}$	$\begin{pmatrix} p_x \\ p_y \end{pmatrix} s_x, \begin{pmatrix} p_x \\ p_y \end{pmatrix} c_x$
$(0, 1)$	$\begin{pmatrix} c_y \\ 0 \end{pmatrix}, \begin{pmatrix} s_y \\ 0 \end{pmatrix}$	$\begin{pmatrix} 0 \\ c_y \end{pmatrix}, \begin{pmatrix} 0 \\ s_y \end{pmatrix}$	$\begin{pmatrix} p_x \\ p_y \end{pmatrix} s_y, \begin{pmatrix} p_x \\ p_y \end{pmatrix} c_y$
$(1, 1)$	$\begin{pmatrix} \frac{1}{k_x} c_x s_y \\ -\frac{1}{k_y} s_x c_y \end{pmatrix}, \begin{pmatrix} \frac{1}{k_x} s_x c_y \\ -\frac{1}{k_y} c_x s_y \end{pmatrix}$ $\begin{pmatrix} \frac{1}{k_y} s_x s_y \\ \frac{1}{k_x} c_x c_y \end{pmatrix}, \begin{pmatrix} \frac{1}{k_y} c_x c_y \\ \frac{1}{k_x} s_x s_y \end{pmatrix}$	$\begin{pmatrix} \frac{1}{k_y} c_x s_y \\ \frac{1}{k_x} s_x c_y \end{pmatrix}, \begin{pmatrix} \frac{1}{k_y} s_x c_y \\ \frac{1}{k_x} c_x s_y \end{pmatrix}$ $\begin{pmatrix} \frac{1}{k_y} s_x s_y \\ -\frac{1}{k_x} c_x c_y \end{pmatrix}, \begin{pmatrix} \frac{1}{k_y} c_x c_y \\ -\frac{1}{k_x} s_x s_y \end{pmatrix}$	$\begin{pmatrix} p_x \\ p_y \end{pmatrix} s_x s_y, \begin{pmatrix} p_x \\ p_y \end{pmatrix} c_x c_y$ $\begin{pmatrix} p_x \\ p_y \end{pmatrix} c_x s_y, \begin{pmatrix} p_x \\ p_y \end{pmatrix} s_x c_y$

Table 3: Decomposition of \mathbf{n} -modes for rectangular systems with periodic boundaries.

Example 4 For the three modes of lowest wave number, Table 3 lists a basis of $T(\mathbf{n})$, $L(\mathbf{n})$ and $P(\mathbf{n})$. Fields are given in a non-normalized form to keep notation short. Corresponding $L(\mathbf{n})$ fields and $P(\mathbf{n})$ fields are LP pairs. Fig. 6 provides examples for T and L -modes.

Modes of $L(\mathbf{n})$ and $T(\mathbf{n})$ are wavelike perturbations of the position space, and, therefore, are similar to the modes that appear in hydrodynamics (see Sec. 8). In particular, when either n_x or n_y vanish, the fields of $L(\mathbf{n})$ and $T(\mathbf{n})$ are, respectively, longitudinal and transverse to the wave vector. This observation is the reason for the names of the two branches in Fig. 5. To stay in line with this now-accepted terminology, we keep it also for the case $n_x \cdot n_y \neq 0$. P -modes are more complex than the other modes, because they depend not only on the positions of the perturbed particles but also on their velocities.

At this point we are able to characterize the spectrum and its multiplicities with only two constants, c_L and c_T , which have the dimension of *velocities*. We shall see in Sec. 7 that these velocities depend on the density of the system, but they are insensitive to the system size, the boundary type, and the aspect ratio. Therefore, it is tempting to think of c_L and c_T as thermodynamic velocities.

5.3 Other aspect ratios and boundary conditions

We summarize here some observations which concern different boundary conditions and degeneracies.

- The Lyapunov spectrum is more degenerate for square systems, for which $k_{(n_x, n_y)} = k_{(n_y, n_x)}$. In this case the multiplicities are doubled with respect to the general case, for which $n_x \neq$

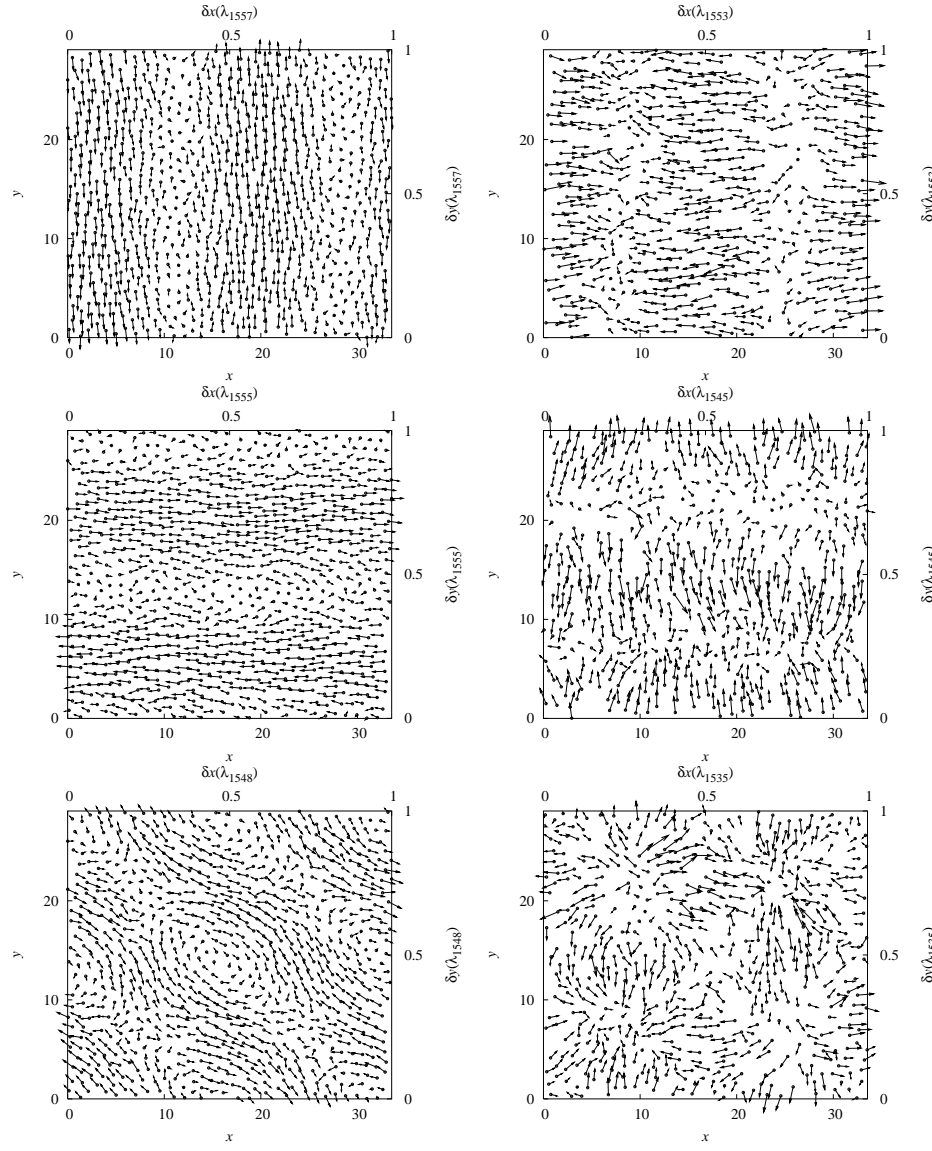


Figure 6: Snapshots of Lyapunov modes for the periodic 780-disk system of Sec. 5. Left, from top to bottom: Transverse modes $T(1,0)$, $T(0,1)$, and $T(1,1)$ belonging to λ_{1557} , λ_{1555} , and λ_{1548} , respectively, of Fig. 5. Right, from top to bottom: Vector fields for longitudinal modes, which belong to the LP pairs $LP(1,0)$, $LP(0,1)$, and $LP(1,1)$, and which are associated with the respective exponents λ_{1553} , λ_{1545} and λ_{1535} , of Fig. 5.

n_y . Other “accidental” degeneracies may occur: for instance, parameters can be found for which $c_T |k_{(1,1)}| = c_L |k_{(1,0)}|$.

ii) Systems with **reflecting** boundaries develop only a subset of the modes encountered so far, which can be found by the following simple, and obvious, rules:

- The fundamental wave vectors are $k_x = \frac{\pi}{L_x}$ and $k_y = \frac{\pi}{L_y}$ (not 2π). Here, L_x and L_y are the *effective* box sizes, obtained from the actual side lengths by subtracting one particle diameter σ .
- The fields of $T(\mathbf{n})$ and $L(\mathbf{n})$ have to satisfy Dirichlet conditions, namely to be tangent to the boundary:

$$\varphi_x(0, y) = \varphi_x(L_x, y) = 0 \quad \text{and} \quad \varphi_y(x, 0) = \varphi_y(x, L_y) = 0.$$

If expressed in terms of sines and cosines, this means that φ_x may contain $\sin(k_x x)$ but not $\cos(k_x x)$, and so on.

- When an L-mode is present, its paired P-mode is always present.

- iii) Hybrid systems with a reflecting boundaries in one direction and periodic boundaries along the other behave as expected [6]: the fundamental wave vectors are chosen according to the boundary type, and the Dirichlet conditions are only applied to one component of the field.
- iv) Narrow systems, for instance those with $L_x \gg \sigma$ and $\sigma < L_y < 2\sigma$,¹⁵ only develop modes with $n_y = 0$ [21]. This follows, since a vector field varying along the y axis cannot be sampled by a single particle. Therefore, the Lyapunov spectrum of such a system is greatly simplified, since the modes are restricted to $L(n_x, 0)$ and $T(n_x, 0)$.

Example 5 Table 4 shows which modes of Table 3 satisfy the Dirichlet condition and are thus present in a system with reflecting boundaries.¹⁶ We stress that such a system has only *two* vanishing Lyapunov exponents which are associated with $\delta\xi_5$ and $\delta\xi_6$ of Table 1. *Therefore, modes appear which are not modulations of zero modes of the system.* The crucial observation here is that even if one of the fundamental symmetries is broken by the boundary condition, the modulation, as defined in Eq. (8), may still satisfy that boundary condition. For example, if we have reflecting boundaries on the walls $\{x = 0\}$ and $\{x = L_x\}$, then any perturbation $A(x, y) = \sin(mk_x x)B(y)$ will be acceptable, whereas, of course, $A(x, y) = \cos(mk_x x)B(y)$ would not.

Systems with reflecting boundaries and narrow systems are easier to study numerically, because the multiplicities of the L, P and T spaces are smaller than in the periodic rectangular case. In particular, the LP(1,1) space has only dimension 2 when the boundaries are reflecting. For

¹⁵Recall that σ is the diameter of the disks.

¹⁶For such a choice of basis vectors the origin of the coordinate system is at the bottom-left corner of the simulation box.

\mathbf{n}	$T(\mathbf{n})$	$L(\mathbf{n})$	$P(\mathbf{n})$
$(1, 0)$	none	$\begin{pmatrix} s_x \\ 0 \end{pmatrix}$	$\begin{pmatrix} p_x \\ p_y \end{pmatrix} c_x$
$(0, 1)$	none	$\begin{pmatrix} 0 \\ s_y \end{pmatrix}$	$\begin{pmatrix} p_x \\ p_y \end{pmatrix} c_y$
$(1, 1)$	$\begin{pmatrix} s_x c_y \\ -c_x s_y \end{pmatrix}$	$\begin{pmatrix} s_x c_y \\ c_x s_y \end{pmatrix}$	$\begin{pmatrix} p_x \\ p_y \end{pmatrix} c_x c_y$

Table 4: Mode decomposition for rectangular systems with reflecting boundaries.

that reason, we illustrate some of the issues below also with the “reflecting-wall version” of the 780-disk system introduced in Fig. 8.

5.4 How to measure P-modes

Contrary to $L(\mathbf{n})$ and $T(\mathbf{n})$, the tangent subspace $P(\mathbf{n})$ *depends on the state that it perturbs*. Moreover, modes of $P(\mathbf{n})$ are not really vector fields, because the velocities of the particles in a typical configuration do not depend smoothly on position. In order to “see” a P-mode, we face two problems:

- i) A typical measured vector of an $LP(\mathbf{n})$ space is a *superposition* of vectors of $L(\mathbf{n})$ and $P(\mathbf{n})$.
- ii) Even when a mode of $P(\mathbf{n})$ is isolated, it is not smooth and does not “look like” a vector field.

We explain our solution to the first problem with the simplest possible example: the $LP(1, 0)$ space for a rectangular system with **reflecting boundaries** (see Sec. 5.3). This space has dimension two and is defined by the two normalized spanning vectors

$$\begin{pmatrix} \varphi_x^L \\ \varphi_y^L \end{pmatrix} = \frac{1}{z_1} \begin{pmatrix} s_x \\ 0 \end{pmatrix}, \quad \begin{pmatrix} \varphi_x^P \\ \varphi_y^P \end{pmatrix} = \frac{1}{z_2} \begin{pmatrix} p_x \\ p_y \end{pmatrix} c_x, \quad k_x = \frac{\pi}{L_x}, \quad (9)$$

where z_1 and z_2 are normalization constants. At any time t , we have two measured modes, ψ^1 and ψ^2 (vectors with $2N$ components, since only the δq part is observed), whose span is (numerically very close to) $LP(1, 0)$. Therefore, there are constants a, b, c, d with

$$\begin{aligned} \varphi^L &= \psi^1 a + \psi^2 b, \\ \varphi^P &= \psi^1 c + \psi^2 d. \end{aligned} \quad (10)$$

Since all these vectors are normalized, one should also have $a^2 + b^2 = c^2 + d^2 = 1$. However, Eq. (10) is over-determined: four constants have to satisfy $4N$ equations. Numerically, we use

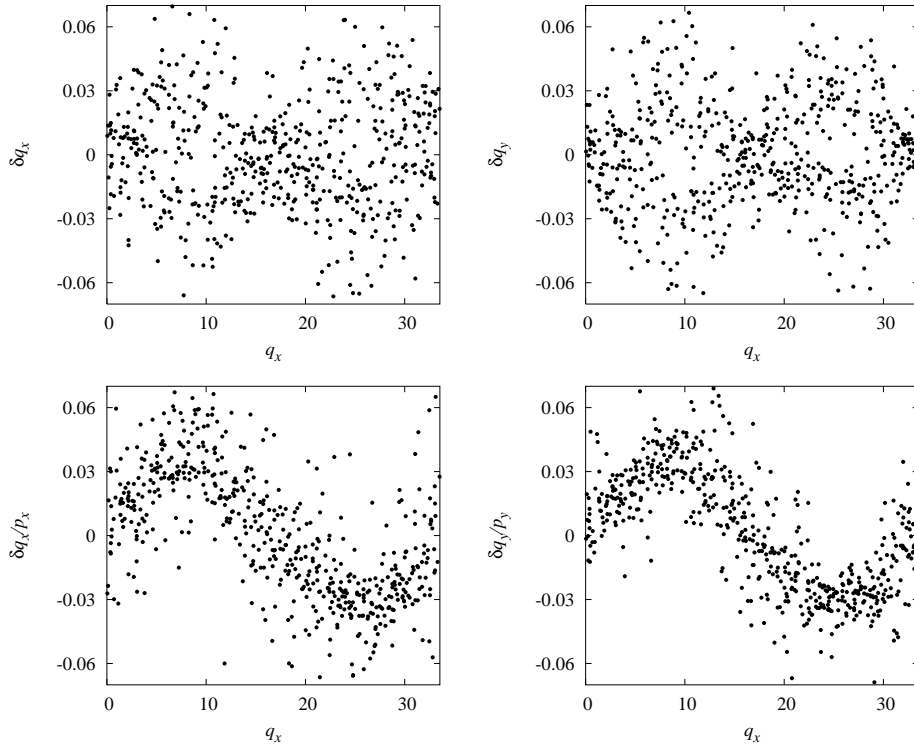


Figure 7: Example for the P-mode reconstruction for the 4-dimensional LP(1,0) space of a system with *periodic boundaries*. Only half of the components are shown, namely those corresponding to s_x . The c_x components are similar. Top row: x and y components of the reconstructed P-mode $\tilde{\varphi}^P \approx ps_x$. Bottom row: the fields $\tilde{\varphi}_x^P/p_x$ and $\tilde{\varphi}_y^P/p_y$ are wavelike again. Note that in the top row one can recognize the sinusoidal envelope.

a least-square method to find the best values for a, b, c and d , which we denote by $\alpha, \beta, \gamma, \delta$.¹⁷ Thus, the measured modes, ψ^1 and ψ^2 , are decomposed according to

$$\begin{aligned}\tilde{\varphi}^L &= \psi^1 \alpha + \psi^2 \beta, \\ \tilde{\varphi}^P &= \psi^1 \gamma + \psi^2 \delta,\end{aligned}$$

where the vectors $\tilde{\varphi}^L$ and $\tilde{\varphi}^P$ are the best-possible LP-pair, φ^L and φ^P , reconstructed from experimental data.

¹⁷It is also possible to use a simple projection $\alpha = \varphi^L \cdot \psi^1$, etc. This method assumes that φ^L and φ^P are orthogonal vectors, which they only are approximately.

Now we can deal with our second problem: whereas the vector $\tilde{\varphi}^L$ is easily recognized as a vector field, the vector $\tilde{\varphi}^P$ is not. However, from (9) we deduce that

$$\begin{pmatrix} \varphi_x^P/p_x \\ \varphi_y^P/p_y \end{pmatrix} = \begin{pmatrix} c_x \\ c_x \end{pmatrix},$$

or, more precisely,

$$\begin{pmatrix} \varphi_{x,j}^P/p_{x,j} \\ \varphi_{y,j}^P/p_{y,j} \end{pmatrix} = \begin{pmatrix} \cos(k_x q_{x,j}) \\ \cos(k_x q_{x,j}) \end{pmatrix}, \quad j = 1, \dots, N. \quad (11)$$

Therefore, both φ_x^P/p_x and φ_y^P/p_y are smooth functions and can be easily visualized.

Remarks

- i) This procedure readily extends to higher-dimensional $LP(\mathbf{n})$ spaces, for instance to the four-dimensional $LP(1, 0)$ space of a periodic system. We take this case as an example to illustrate in Fig. 7 our method of mode reconstruction: from the four measured modes the analogue to Eq. (10) generates four spanning vectors, namely two L-modes (one of which is shown at the top-right position of Fig. 5) and two P-modes. The x and y components of one of the P-modes, namely $\tilde{\varphi}^P \approx ps_x$, are shown in the top row of Fig. 7. No smooth functions are recognized. However, after dividing by the momentum components, $p_{x,j}$ and $p_{y,j}$, as required by (11), the figures for the fields $\tilde{\varphi}_x^P/p_x$ and $\tilde{\varphi}_y^P/p_y$ in the bottom row of Fig. 7 clearly display the expected s_x -dependence.
- ii) Division by $p_{x,j}$ or $p_{y,j}$ in (11) is numerically unstable when particle j has a very small momentum along a coordinate axis. We avoid this by multiplying instead by $p_{x,j}/(p_{x,j}^2 + \varepsilon)$, where $\varepsilon \ll 1$. One could also ignore particle j in this case and only sample the field at those points where both $p_{x,j}$ and $p_{y,j}$ are not too small.

6 Dynamics of the modes

Remark The interested reader can look up animated pictures on the web at the address <http://theory.physics.unige.ch/modes/>.

In this section we turn to the “dynamics of the modes” and study what has been called the velocity of the longitudinal modes [2, 5, 7]. This might clarify hydrodynamic theories [4, 5, 7], which are mostly based on a partial classification of the modes. In numerical simulations, the *transverse* modes are stationary in space and time: although the particles move, the vector-field of the mode does not. In other words, at any instant of time, the vector field of a T-mode does not move (up to a small jitter due to numerical noise).

For *longitudinal* modes, however, one seems to observe [19] a propagation in the direction of the wave vector.¹⁸ Using the geometrical picture developed above, we can interpret this motion

¹⁸when either n_x or n_y vanish, for instance in the $L(1, 0)$ or $L(0, 1)$ space.

and also explain why no propagation is observed for the LP dynamics in systems with reflecting boundaries as demonstrated in Fig. 8 below.

Since multiplicities are not so essential here, we illustrate the interpretation for the (simpler) LP(1,0) space of a rectangular system with reflecting boundaries (dimension 2). In Sec. 5.4 we pointed out that at any given time t , where the state is ξ_t , the measured modes $\psi^1(t)$ and $\psi^2(t)$ are combinations of the two spanning vectors $\varphi^L(\xi_t)$ and $\varphi^P(\xi_t)$. We re-write Eq. (10) in matrix form, but now with explicit time dependence:

$$(\varphi^L(\xi_t), \varphi^P(\xi_t)) = (\psi^1(t), \psi^2(t)) \cdot Q(t), \quad Q(t) = \begin{pmatrix} a(t) & b(t) \\ c(t) & d(t) \end{pmatrix}.$$

Therefore, the dynamics of the modes reduces to that of the 2×2 matrix $Q(t)$. In our simulations we keep the spanning vectors orthonormal. Since (in the experiment) the two fields φ^L and φ^P are also (nearly) orthogonal¹⁹, the matrix $Q(t)$ is close to a **rotation** matrix (that is $c \simeq -b$, $d \simeq a$, and $a^2 + b^2 \simeq 1$). Therefore, the dynamics in the two-dimensional subspace is well described by a phase $\phi(t) = \arctan(b(t)/a(t))$.

LP-dynamics in 2 dimensions: *The matrix $Q(t)$ is a rotation with **constant** angular velocity ω_n . This velocity is proportional to the wave number k_n , namely*

$$\phi(t) = \omega_n t = v k_n t.$$

Here, v is the product of a frequency and a wavelength and, therefore, is a velocity. According to the simulations, v depends only on the density of the system.

Example 6 In Fig. 8 we demonstrate this rotation in the LP(1,0) space of a system with reflecting boundaries. Snapshots of the two measured fields at consecutive times show the rotation of the two vectors between the L and the P direction.

A theory explaining this dynamics is not available at the moment, although a similar rotation is present in the approach of de Wijn and van Beijeren [7].

Remark 7 The velocity $v = \omega_n/|k_n|$ has been interpreted earlier [19] as the phase velocity of a traveling wave in physical space. In Appendix B we demonstrate how the two interpretations can be reconciled. The definitions given above allow us to apply the same concepts also to the LP-dynamics of systems with reflecting boundaries, although they do not show traveling but standing waves.

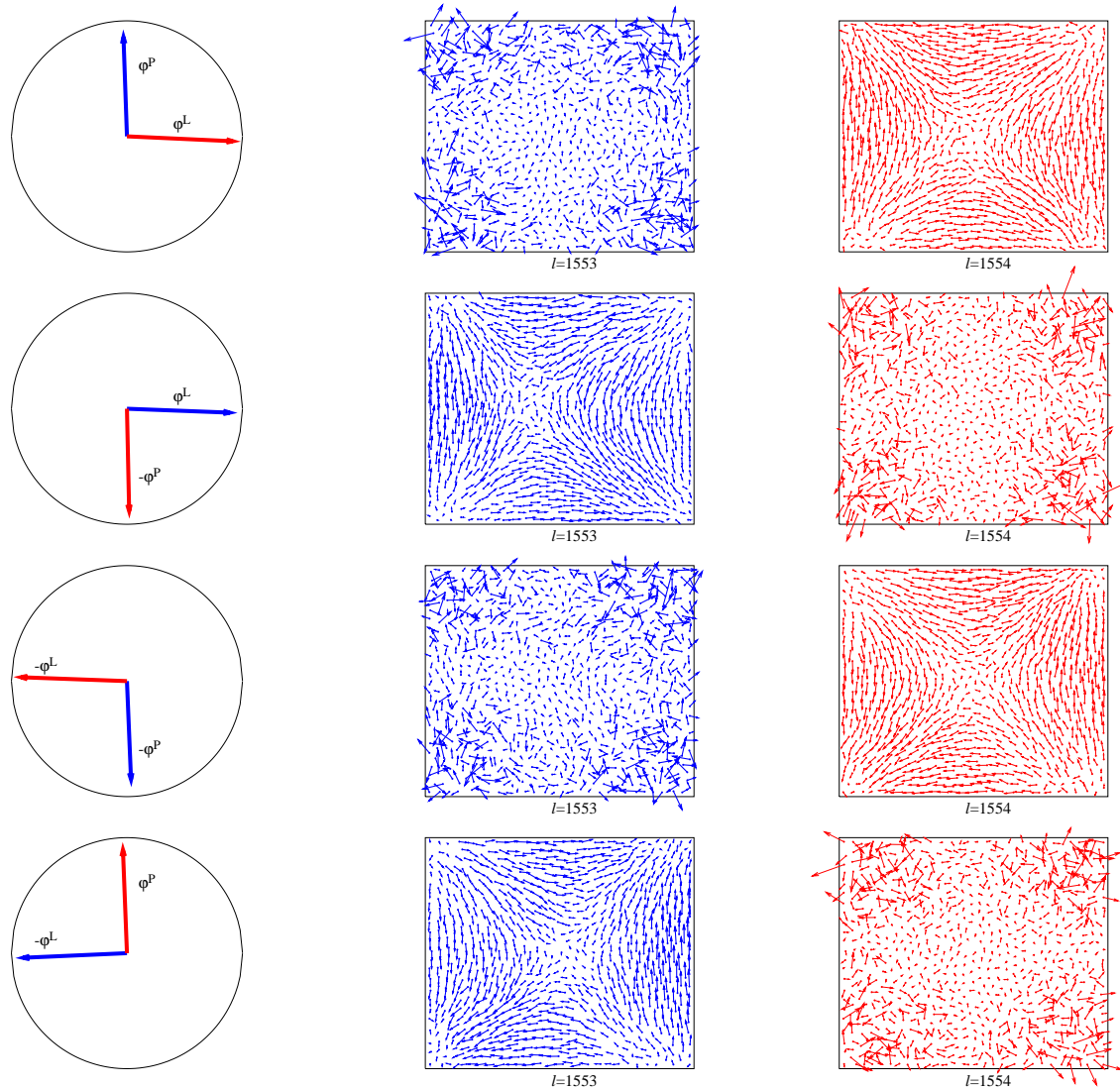


Figure 8: LP(1,1) dynamics for a system of 780 disks in a box with an aspect ratio 0.867, a density 0.8, and with *reflecting* boundaries. Left: coordinates of the measured fields in the “standard basis” of LP(1,1). The (unit) circle is nearly reached, showing that indeed ψ^1 and ψ^2 span the same subspace as φ^L and φ^P . Center and right: the measured fields $\psi^1(t)$ and $\psi^2(t)$. The rows from top to bottom are consecutive snapshots separated by time steps of $\Delta t = 3.20$, which corresponds to a phase shift of $\pi/2$ in the LP(1,1) rotation.

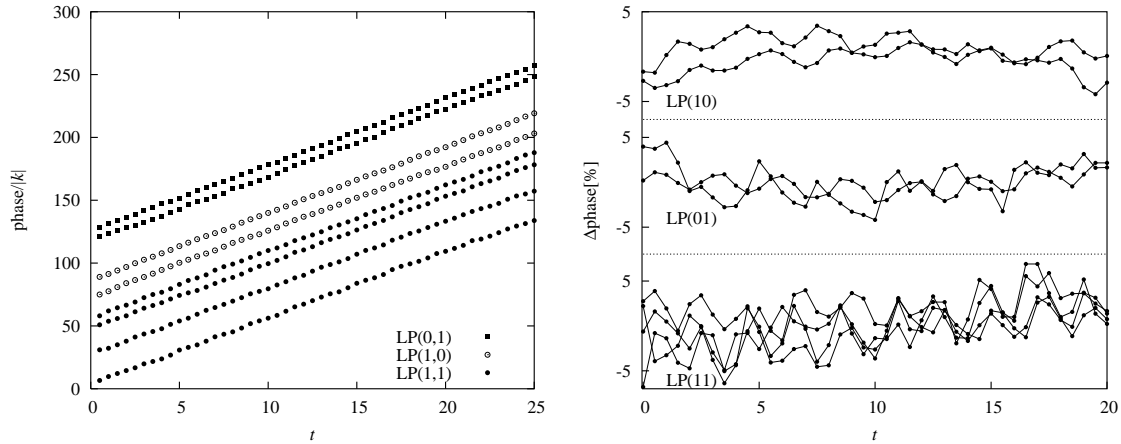


Figure 9: Rotations of various LP pairs for the 780-disk system of Fig. 1. Left: Time dependence of the phase. For clarity, the phases for different modes are separated by multiples of $2\pi/|k_n|$. Right: The fluctuations around the constant velocity (in percent of 2π). For details we refer to the main text.

Next, we consider the dynamics for the general case of a $2d$ -fold degenerate LP(\mathbf{n}) space. As explained in Sec. 5, an LP(\mathbf{n}) space is defined by a spanning set of d longitudinal modes, $\varphi_1^L, \dots, \varphi_d^L$, and d P-modes, $\varphi_1^P, \dots, \varphi_d^P$, where each pair $(\varphi_k^L, \varphi_k^P)$ is an LP pair. The following description is valid for any type of boundary conditions:

Dynamics in LP(\mathbf{n}): *The dynamics in LP(\mathbf{n}), when restricted to a two-dimensional subspace spanned by an LP pair*

$$\text{Span}\{\varphi_k^L, \varphi_k^P\},$$

is a two-dimensional rotation at a constant angular velocity $\pm\omega_{\mathbf{n}}$, where $\omega_{\mathbf{n}} = v k_{\mathbf{n}}$, with v independent of \mathbf{n} .

Example 8 The LP dynamics for higher-dimensional spaces is illustrated in Fig. 9. In the following we concentrate on LP(1,1). This space has dimension 8, that is four LP pairs. Generically, a measured mode has a non-vanishing projection onto all four LP pairs, and four different phases can be defined. The four time series of phases for LP(1,1) in Fig. 9 belong to different projections of the *same* mode.

¹⁹The scalar product $\varphi^L \cdot \varphi^P = \sum_{j=1}^N \cos(k_x q_{j,x}) \sin(k_x q_{j,x}) p_{j,x}$ a priori does not vanish. However, as the simulations show, it is of the same order as $\sum_{j=1}^N \cos(k_x q_{j,x}) \sin(k_x q_{j,x})$, which is also small and non-vanishing due to the uneven spacing of the particles.

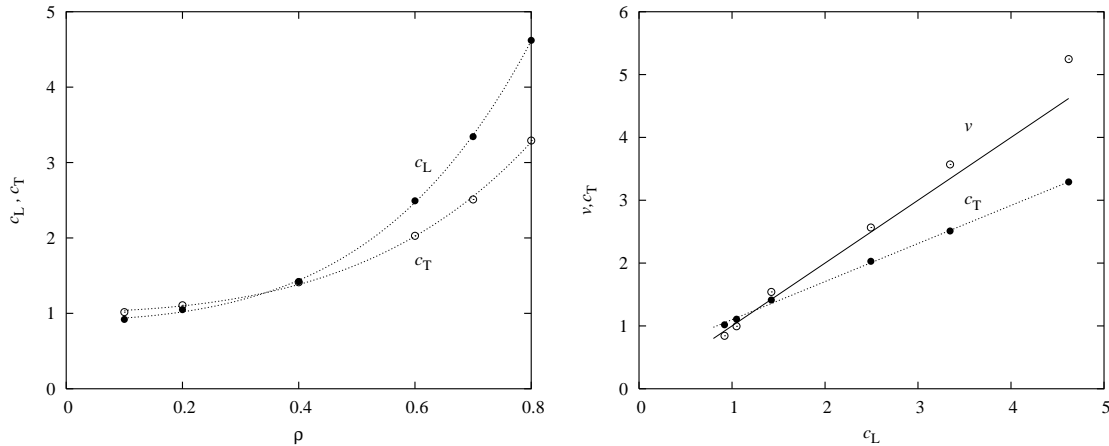


Figure 10: Slopes of the transverse and longitudinal branches c_T and c_L of Fig. 5, and of phase velocity v . The simulations are for a system containing $N = 780$ particles in a rectangular periodic box with a fixed aspect ratio $L_y/L_x = 0.867$. Left: c_T and c_L as a function of the particle density ρ . The smooth lines are polynomial fits, $c_L = 1.02 + 1.84\rho^2 + 2.62\rho^4$, and $c_T = 0.91 + 2.45\rho^2 + 5.2\rho^4$. Right: Almost linear relations between all three quantities.

7 Influence of geometry and system size

In this section we study what influence the density, aspect ratio, and boundary conditions have on c_T , c_L , and v . The density dependence is significant. Unfortunately, we do not have any explanation for this fact. In particular, comparisons with the sound velocity [20], with the mean free path, and with similar quantities, do not suggest simple relationships. Thus, these questions have to await further studies.

The results of our simulations are summarized in Fig. 10. In the left panel, c_L and c_T , defined in Sec. 2, are shown as functions of ρ , and on the right-hand side v and c_T are plotted as functions of c_L . There are two observations which are of interest: First, as seen in the left panel, c_T and c_L cross for lower densities. Thus, the intuitively natural conjecture, $c_L \geq c_T$, is not supported by the numerical evidence. Second, the three “velocities” c_T , c_L , and v are almost linearly related. In particular, the phase velocity v agrees rather well with c_L for fluid densities $\rho < 0.6$ (see the full line in the right-hand side of Fig. 10), thus lending support to referring to the curves $\lambda(k)$ as “dispersion relations”.

On the left-hand side of Fig. 11 we plot the longitudinal and transverse dispersion relations for a moderately-dense gas with a density $\rho = 0.4$. The full and open points are for systems with periodic and reflecting boundaries, respectively. In all cases, λ was determined from the lowest step of the Lyapunov spectrum for the system, for which the aspect ratio varied between

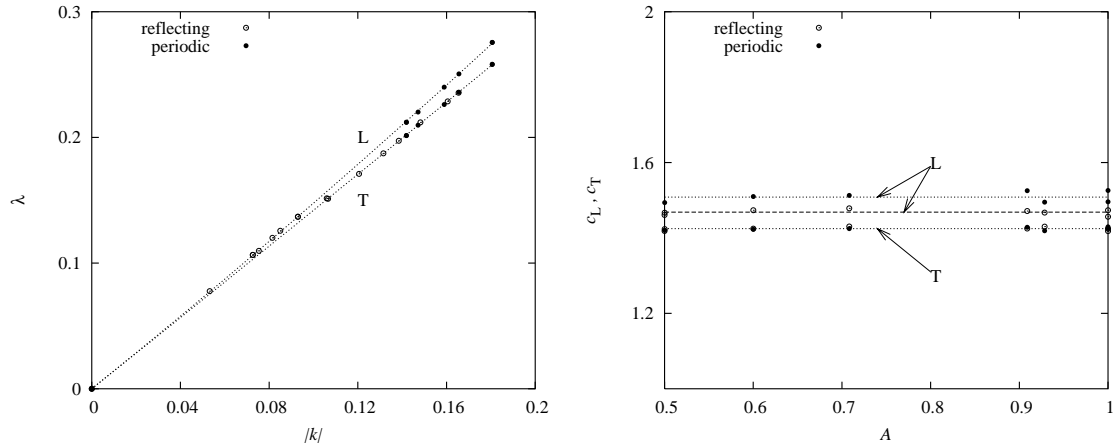


Figure 11: Simulation results for a hard-disk gas with a density $\rho = 0.4$. The full and open points refer to periodic and reflecting boundary conditions, respectively. Left: The smallest positive Lyapunov exponent for T and L-modes, respectively, as a function of the wave-number k . The curves for periodic and reflecting boundary conditions agree. To the second order in k , a fit to the data gives $c_L = 1.422k + 0.55k^2$ and $c_T = 1.412k + 0.086k^2$. Right: The slopes, c_L and c_T , plotted as a function of the aspect ratio A of the simulation box. The data for periodic and reflecting boundaries agree for c_T (indicated by the full line labeled T), whereas there is a noticeable difference for c_L (indicated by the dashed and dotted lines with the label L).

0.5 and 1, and the particle number between 400 and 800. The figure demonstrates that periodic and reflecting boundary conditions give the same $\lambda(k)$. We have experimentally verified (but not shown here) that the same is true also for larger and lower densities.

The situation becomes more complicated when we consider the slopes of these curves, c_L and c_T , as we do on the right-hand side of Fig. 11. There we plot them as a function of the aspect ratio $A = L_y/L_x$, where, again, full and open points refer to periodic and reflecting boundaries, and the labels L and T point to the longitudinal and transverse branches. One observes that in all cases c_L and c_T are independent of the aspect ratio and, thus, of the geometry, as long as the box does not degenerate to a narrow channel [21]. Furthermore, c_T , agrees well for periodic and reflecting boxes (full line), but c_L does not (dashed and dotted lines). The reason for this behavior is that the dispersion relations are not strictly linear as we have pointed out already in a footnote in Sec. 2. A fit to the points in the left panel of Fig. 11 reveals, that the term proportional to k^2 is much larger for L than for T and is responsible for the observed split of c_L due to the different boundary conditions.²⁰ This nonlinearity has no noticeable influence on the classification and

²⁰The smallest wave number k for periodic boundaries is given by $2\pi/L$, where L is a dimension of the box. For reflecting boundaries, k is given by π/L , where L is an effective box size, namely the size reduced by a particle diameter σ .

description of the Lyapunov modes in this paper and has been accordingly ignored.

8 Perturbation of the local hydrodynamic fields

There is a general expectation that the Lyapunov modes should be associated with hydrodynamic quantities, and several papers point in this direction [3, 4, 5, 6, 7]. It should be noted, however, that none of these studies has reached a totally convincing interpretation, and, furthermore, it is obvious from this body of work that the LP-modes are more difficult to explain than the T-modes. Here, we add to this a simple phenomenological interpretation which might be helpful in the future.

To understand the hydrodynamic nature of the modes, we calculate how they perturb certain hydrodynamic fields. Consider a general transformation T of the one-particle phase space $\mu \equiv [0, L_x) \times [0, L_y) \times \mathbf{R}^2$ given by

$$T : \begin{cases} r \mapsto r' = r + \varepsilon \delta\xi(r, v) \\ v \mapsto v' = v + \varepsilon \delta\eta(r, v) \end{cases},$$

and f a probability density over μ . If ε is infinitesimal, then the new probability density is $f' = f + \varepsilon \delta f$, where

$$\delta f = -f (\nabla_r \cdot \delta\xi + \nabla_v \cdot \delta\eta) - \nabla_r f \cdot \delta\xi - \nabla_v f \cdot \delta\eta, \quad (12)$$

see Appendix A. Since we study equilibrium dynamics, we assume, furthermore, that f is the Boltzmann distribution²¹. By Sec. 4.1 we also have $\delta\eta = C\delta\xi$, and, therefore, (12) simplifies to

$$\delta f = -f (\nabla_r \cdot \delta\xi + C\nabla_v \cdot \delta\xi - Cv \cdot \delta\xi).$$

We define the variations of the three hydrodynamic fields (density ρ , momentum u , and energy E) by

$$\delta\rho(r) = \int dv \delta f(r, v), \quad \delta u(r) = \int dv \delta f(r, v) v, \quad \delta E(r) = \int dv \delta f(r, v) |v|^2.$$

For each of the three types of modes, one can compute these quantities as a function of the scalar modulation A introduced in (8). The results are given in Table 5. Since $\Delta A = -k_n^2 A$, we note that the scalar fields $\delta\rho$ and δE are proportional to the initial scalar modulation A . Note also that the energy field is only affected by the L and P-modes but not by the T-mode.

²¹with $k_B T = 1$ as in the simulations

mode	$\delta\xi$	$\delta\rho$	δu	δE
T	$\nabla \wedge A$	0	$\nabla \wedge A$	0
L	∇A	ΔA	∇A	ΔA
P	$v A$	0	∇A	A

Table 5: Modulations of the hydrodynamic fields (multiplicative constants are omitted)

9 Conclusions

The picture developed in this paper is for two-dimensional hard disks, but the method is sufficiently geometric and general to allow easy extensions to other systems:

For example, the generalization to three-dimensional hard disks is straightforward. The existence of L and T-modes for this case has been confirmed by computer simulation [20]. Recently, Lyapunov modes were also found for two-dimensional soft-particle systems interacting either with a Weeks-Chandler-Anderson potential [22] or a Lennard-Jones potential [23, 24]. It would also be interesting to extend the work to, say, circular geometries. Another extension concerns linear molecules such as hard dumbbells in a periodic box [1, 12]. In this case two qualitatively different degrees of freedom play a role, translation and rotation. The existence of modes has already been demonstrated in this case.

We have ended our wanderings through the rich landscape of Lyapunov modes. To summarize, we have carefully identified and analyzed the modes, giving a beginning of a theoretical classification. Furthermore, we have seen that the Lyapunov exponents and the phase velocity of the LP-modes seem to be functions of the density alone. In particular, they are practically independent of the aspect ratio of the box (and, where applicable, also insensitive to the boundary conditions).

10 Acknowledgments

Financial support from the Austrian Science Foundation (FWF), project P15348, and the Fonds National Suisse is gratefully acknowledged.

A Transformation of the one-particle distribution

Let f be a given distribution. For $\Gamma \subset \mu$, we have

$$F(\Gamma) \equiv \text{Prob}(\text{one particle } \in \Gamma) = \int_{\Gamma} dr dv f(r, v).$$

The transported probability F' is defined by $F'(\Gamma') = F(\Gamma)$, where $\Gamma' = T(\Gamma)$. We shall compute its density f' . In the integral

$$F(\Gamma) = \int_{T^{-1}(\Gamma')} dr dv f(r, v) , \quad (13)$$

we change the variables to $(r', v') = T(r, v)$. To first order in ε , we have

$$T^{-1} : \begin{cases} r' \mapsto r = r' - \varepsilon \xi(r', v') \\ v' \mapsto v = v' - \varepsilon \eta(r', v') \end{cases} ,$$

so (13) becomes

$$F(\Gamma) = \int_{\Gamma'} dr' dv' \det[DT^{-1}|_{r', v'}] f(r' - \varepsilon \xi(r', v'), v' - \varepsilon \eta(r', v')) . \quad (14)$$

The determinant is

$$\begin{aligned} \det[DT^{-1}|_{r', v'}] &= \det \begin{pmatrix} \text{Id} - \varepsilon D_r \xi & -\varepsilon D_v \xi \\ -\varepsilon D_r \eta & \text{Id} - \varepsilon D_v \eta \end{pmatrix} \Big|_{r', v'} \\ &= 1 - \varepsilon [\nabla_r \cdot \xi + \nabla_v \cdot \eta]_{r', v'} . \end{aligned} \quad (15)$$

To first order in ε , we obtain with (14) and (15)

$$\begin{aligned} F(\Gamma) &= F(\Gamma') - \varepsilon \int_{\Gamma'} dr' dv' f(r', v') [\nabla_r \cdot \xi + \nabla_v \cdot \eta]_{r', v'} \\ &\quad - \varepsilon \int_{\Gamma'} dr' dv' [\nabla_r f \cdot \xi + \nabla_v f \cdot \eta]_{r', v'} , \end{aligned}$$

which is equivalent to (12).

B Traveling waves of LP dynamics

We consider the LP(1, 0) space of a rectangular system with periodic boundary conditions, defined by the four spanning vectors

$$\varphi_{\sin}^L = \begin{pmatrix} s_x \\ 0 \end{pmatrix} , \quad \varphi_{\cos}^P = \begin{pmatrix} p_x \\ p_y \end{pmatrix} c_x , \quad \varphi_{\cos}^L = \begin{pmatrix} c_x \\ 0 \end{pmatrix} , \quad \varphi_{\sin}^P = \begin{pmatrix} p_x \\ p_y \end{pmatrix} s_x .$$

We take an initial tangent vector

$$\delta \xi_0 = a \varphi_{\sin}^L + b \varphi_{\cos}^P . \quad (16)$$

After a time $\tau = 2\pi/(4\omega_n)$, the vector is transformed to

$$\delta \xi_\tau = a \varphi_{\cos}^P + b \varphi_{\sin}^L . \quad (17)$$

Assume that a and b are more or less equal. Then (16) will resemble a sinus, with much “noise” due to the P component, while (17) will look more like a cosine. In the dynamics leading from (16) to (17) a kind of “traveling wave” is therefore visible, which seems to cover a distance $2\pi|k_n|^{-1}$ in a time $2\pi\omega_n^{-1}$, thus “moving” at velocity $v = \omega_n/|k_n|$. In actual simulations, we cannot expect typical vectors to have a phase difference of $\frac{\pi}{2}$ between their φ_{\sin}^L and φ_{\cos}^L components, as in our example. Therefore, the observed wave displacement as seen in [20, 19] has the shape of “steps” in a space-time diagram, with an average slope equal to v .

References

- [1] Lj. Milanović, H.A. Posch, and Wm. G. Hoover, “What is ‘Liquid’? Understanding the States of Matter”, *Molec. Phys.*, **95**, 281 - 287 (1998).
- [2] H. A. Posch and R. Hirschl, “Simulation of Billiards and of Hard-Body Fluids”, p. 269 in *Hard Ball Systems and the Lorenz Gas*, edited by D. Szász, Encyclopedia of the mathematical sciences **101**, Springer Verlag, Berlin (2000).
- [3] J.-P. Eckmann and O. Gat, “Hydrodynamic Lyapunov modes in translation-invariant systems”, *J. Stat. Phys.* **98**, 775 (2000).
- [4] S. McNamara and M. Mareschal, “The Lyapunov Spectrum of granular gases”, *Phys. Rev. E* **63**, 061306 (2001)
- [5] S. McNamara and M. Mareschal, “On the origin of the hydrodynamic Lyapunov modes”, *Phys. Rev. E* **64**, 051103 (2001).
- [6] T. Taniguchi and G. P. Morriss, “Boundary effects in the stepwise structure of the Lyapunov spectra for quasi-one-dimensional systems”, *Phys. Rev. E* **68**, 026218 (2003).
- [7] A. de Wijn and H. van Beijeren, “Goldstone modes in Lyapunov spectra of hard sphere systems”, *Phys. Rev. E*, submitted.
- [8] Ch. Forster, R. Hirschl, H. A. Posch, and Wm. G. Hoover, “Perturbed phase-space dynamics of hard-disk fluids”, *Physica D* **187**, 294 (2004)
- [9] N. Simányi and D. Szász, “Hard ball systems are completely hyperbolic”, *Ann. Math.* (2), 149 (1999)
- [10] V. I. Oseledec, “A multiplicative ergodic theorem. Lyapunov characteristic numbers for dynamical Systems”, *Trudy Mosk. Mat. Obshch.* **19**, 179 [Moscow Math. Soc. **19**, 197 (1968)].
- [11] J.-P. Eckmann and D. Ruelle, “Ergodic theory of chaos and strange attractors”, *Rev. Mod. Phys.* **57**, 617 (1985).

- [12] Lj. Milanović and H. A. Posch, “Localized and delocalized modes in the tangent-space dynamics of planar hard dumbbell fluids”, *J. Mol. Liquids*, **96-97**, 221 (2002).
- [13] Ch. Dellago, H. A. Posch, and Wm. G. Hoover, “Lyapunov instability of hard disks in equilibrium and nonequilibrium steady states”, *Phys. Rev. E* **53**, 1485 (1996).
- [14] G. Benettin, L. Galgani, A. Giorgilli, J.-M. Strelcyn, *Meccanica* **15**, 21 (1980).
- [15] I. Shimada and T. Nagashima, *Prog. Theor. Phys.* **61**, 1605 (1979).
- [16] M. Wojtkowski, “Systems of classical interacting particles with non-vanishing Lyapunov exponents” in *Lyapunov exponents (Oberwolfach, 1990)*, Lecture Notes in Math. 1486, Springer (1991).
- [17] L. Bunimovich, C. Liverani, A. Pellegrinotti, and Y. Suhov, “Ergodic systems of n balls in a billiard table”, *Commun. Math. Phys.* **146**, 357 (1992).
- [18] Ch. Dellago and H. A. Posch, “Kolmogorov-Sinai entropy and Lyapunov spectra of a hard sphere gas”, *Physica* **D240**, 68 (1997).
- [19] Ch. Forster, R. Hirschl, and H. A. Posch, “Analysis of Lyapunov modes for hard-disk systems”, *Proc. of ICMP 2003*.
- [20] R. Hirschl, “Computer simulation of hard-disk systems: “Lyapunov modes” and stochastic color conductivity”, diploma thesis, University of Vienna, 1999.
- [21] Ch. Forster, D. Mukamel, and H. A. Posch, “Hard disk in narrow channels”, submitted to *Phys. Rev. E*, (2004).
- [22] Ch. Forster and H. A. Posch, “Lyapunov modes for soft-disk fluids” submitted (2004).
- [23] G. Radons and H. Yang, *Phys. Rev. Lett.*, “Static and dynamic correlations in many-particle Lyapunov vectors”, submitted to *Phys. Rev. Lett.*, (2004).
- [24] H. Yang and G. Radons, “Lyapunov instabilities of Lennard-Jones fluids”, *Phys. Rev. E*, submitted (2004).